Numerical study of pattern formation in miscible rotating Hele-Shaw flows

Ching-Yao Chen[1,*] and Chen-Hua Chen[1,2]
[1]*Department of Mechanical Engineering, National Yunlin University of Science & Technology, Yunlin, Taiwan, Republic of China*
[2]*Department of Automation Engineering, Nan-Kai Institute of Technology, Nantou, Taiwan, Republic of China*

José A. Miranda[†]
Department of Physics, University of Florida, P.O. Box 118440, Gainesville, Florida 32611-8440, USA
(Received 15 August 2005; published 18 April 2006)

The dynamics of the diffusing interface separating two miscible fluids in a rotating Hele-Shaw cell is studied by intensive and highly accurate numerical simulations. We perform numerical experiments in a wide range of parameters, focusing on the influence of viscosity contrast and Korteweg stresses on the shape of the interfacial patterns. A great variety of morphological behaviors is systematically introduced, and a wealth of interesting phenomena related to finger competition dynamics, filament stretching, and interface pinch off are reveal. Our simulations exhibit miscible patterns that bear a strong resemblance to their immiscible counterparts for larger Korteweg stresses. The quantitative equivalence between such stresses and the usual immiscible surface tension is studied. The concept of an effective interfacial tension is considered, allowing the direct and precise calculation of the important fingering properties under miscible circumstances. Our results show excellent agreement with existing experiments and simulations for corresponding immiscible displacements. This agreement refers to a striking similarity between miscible and immiscible pattern morphologies, and also to an accurate prediction for the typical number of miscible fingering structures formed. Our findings suggest that the effective interfacial tension is both qualitatively and quantitatively equivalent to its immiscible counterpart.

DOI: 10.1103/PhysRevE.73.046306 PACS number(s): 47.54.−r, 47.20.Ma, 47.11.−j, 64.75.+g

I. INTRODUCTION

Since the seminal work by Schwartz [1] many groups have studied viscous flow and interfacial pattern formation in rotating Hele-Shaw cells [2–18]. The problem consists of an initially circular fluid droplet, surrounded by a fluid of smaller density, confined in the narrow gap between two parallel glass plates (Hele-Shaw cell). The system rotates around an axis perpendicular to the plane of the flow, so that the interfacial instability is driven by centrifugal forces acting on the fluid-fluid interface. This moving boundary problem is a variation of the classical viscosity-driven Saffman-Taylor instability [19], in which perturbations at the interface now arise primarily due to the difference in density between the fluids. It is well known [5,6,11,16] that the most important and usual morphological features in the rotating Hele-Shaw situation with *immiscible* fluids can be properly described in terms of two dimensionless parameters: the viscosity contrast A (dimensionless viscosity difference), and an immiscible surface tension coefficient which is a measure of capillary forces relative to centrifugal forces in the problem.

A great deal of attention has been paid to the study of the development of interfacial patterns in rotating Hele-Shaw cells. Over the last few years the problem has been studied analytically, numerically, and experimentally. On the analytical side, researchers have performed linear [1–4] and weakly nonlinear [5,6] stability analyses of the problem. Other groups have studied particular families of exact solutions for rotating drops and fluid annulus [7–11]. Intensive numerical simulations have been employed to examine the low viscosity contrast limit [12] with immiscible fluids (using boundary integral techniques), and the high A limit in which the fluids involved are miscible [13,14] (using spectral methods), or immiscible but magnetic [15] (using a conformal method approach). A more recent numerical study used phase-field simulations [11] to investigate the immiscible case for $A \geqslant 0$, but only very recently the full range of viscosity contrasts ($-1 \leqslant A \leqslant +1$) has been systematically analyzed through a numerical vortex sheet formalism [16]. Experimental investigations focus on the high [2] and low [12] positive viscosity contrast flows of immiscible drops, and the radial immiscible displacement of a rotating fluid annulus, in stable [17] and unstable [18] regimes.

Very recent numerical simulations [16] based on the vortex sheet representation [20] for immiscible rotating Hele-Shaw flow have verified that the viscosity contrast A plays a crucial role in determining the pattern morphology, in the sense that changes in its *magnitude* and *sign* result in fingering patterns presenting very different typical lengths and widths. It has been shown that finger competition dynamics and the occurrence (and location) of interfacial pinch off events are dramatically modified as A varies. Generally speaking, it has been found that by varying A from -1 to $+1$ the shape of the emerging fingers change from wide petallike structures when $A=-1$, to thin filamented arms presenting bulbous ends when $A=0$, and finally to branched, backbone structures with nearly constant widths when $A=+1$. The position of pinch off moves from the region closer to the rotation axis ($A=-1$) towards the tip of the finger ($A=0$). In

*Email address: chingyao@yuntech.edu.tw
[†]On leave from Departamento de Física, LFTC, UFPE, Brazil. Email address: jme@df.ufpe.br

addition, it has been observed that pinch off events are not systematically favored when $A=+1$. As far as finger competition dynamics is concerned, increasingly larger values of the magnitude of $A<0$ ($A>0$) lead to enhanced competition among outward (inward) fingers. It has been also verified that competition is significantly suppressed when $A\to 0$. Regarding the role of the surface tension coefficient, it basically sets the typical number of fingers formed at the onset of the instability, where smaller values of usual immiscible surface tension lead to more vigorous fingering [6,12,16].

Although the patterns simulated in Ref. [16] agree extremely well with the corresponding structures obtained experimentally in the limits of high [2] and low [12] positive A (mainly when the cell is prewetted), experimental studies examining the cases with $A\leqslant 0$, and covering a wide range of values for the surface tension coefficient are still not available in the literature. With respect to this point, the theoretical study of the rotating Hele-Shaw problem with *miscible* fluids (zero interfacial tension situation) can be very useful in checking the validity of the predictions made in the immiscible case [16]. As discussed throughout this work, a link between miscible displacement and immiscible flow can be provided by the introduction of stresses arising as a result of concentration gradients at the diffusing interface. A number of theoretical [14,21–34] and experimental [35–41] works with miscible fluids show strong evidence for the fact that such stresses, known as Korteweg stresses [42], may significantly affect the behavior of the mixing interface, introducing surface tensionlike effects into the miscible system. Despite all these qualitative evidence, a more quantitative study connecting Korteweg stresses and usual surface tension is still lacking. Moreover, the miscible problem in rotating Hele-Shaw cells is particularly interesting since it potentially gives rise to an unexplored phenomenology, which is likely to result in quite different pattern morphologies and distinct types of interfacial behaviors not revealed in the immiscible case. In addition, it is clearly desirable to be able to systematically study the combined role of viscosity contrast, miscibility, and Korteweg stresses in determining the shape of the rotating diffusing interface at fully nonlinear stages. In light of this, it is the purpose of this paper to address all these issues, both qualitatively and quantitatively, through intensive and highly accurate numerical simulations.

The rest of the paper is organized as follows: Section II formulates our theoretical approach, presents the governing equations, and describes the numerical scheme we have implemented to study the rotating Hele-Shaw system with miscible fluids. Section III discusses the results, both in qualitative and quantitative terms. Section III A focus on the analysis of the influence of viscosity contrast and Korteweg stresses, and reveals a great variety of morphological behaviors as these parameters are varied. In particular, it is shown that the shape of the miscible patterns and their finger competition dynamics behave very similarly to the immiscible case for stronger Korteweg stresses. Section III B seeks for more quantitative results: by defining the miscible equivalent of the usual immiscible surface tension, our theoretical approach leads to a quantitative relationship between the number of fingers formed in fully nonlinear stages and the value of such control parameter. Finally, our numerical results are systematically compared to simulations and experiments performed in its immiscible counterpart. A striking similarity is found between our numerical miscible results and other numerical and experimental studies restricted to the immiscible case. Our main conclusions are summarized in Sec. IV.

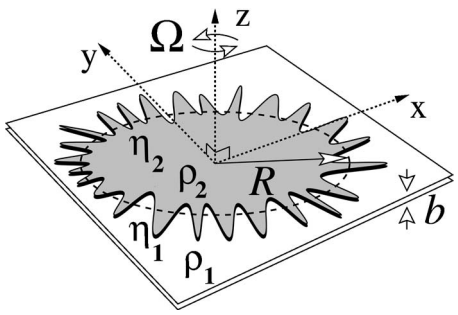

FIG. 1. Diagrammatic representation of the rotating Hele-Shaw cell with miscible fluids and the (x,y,z) coordinate system.

II. NUMERICAL APPROACH AND GOVERNING EQUATIONS

Consider a Hele-Shaw cell of gap thickness b containing two miscible, incompressible, viscous fluids (see Fig. 1). Denote the densities and viscosities of the inner and outer fluids, respectively as ρ_2, η_2 and ρ_1, η_1. We assume that the inner fluid is more dense ($\rho_2>\rho_1$), however it can be either more or less viscous than the outer fluid. We define our Cartesian coordinate system (x,y,z) in such a way that its origin is located at the center of the droplet. The lower (upper) plate is located at $z=0$ ($z=b$), where the z axis points in the direction perpendicular to the plates. The cell rotates with constant angular velocity Ω about the z axis. Initially, the mixing interface is circular and has radius R. As time advances, centrifugal effects take place and the fluids begin to mix diffusively, giving rise to complex interfacial patterns.

The evolution of the diffusing interface in such rotating Hele-Shaw cell is governed by the following set of equations [2,12,13,23]

$$\nabla\cdot\mathbf{u}=0, \tag{1}$$

$$\nabla(p+Q)=-\frac{12\eta}{b^2}\mathbf{u}+\rho\Omega^2\mathbf{r}+\nabla\cdot[\hat{\delta}(\nabla c)(\nabla c)^T], \tag{2}$$

$$\frac{\partial c}{\partial t}+\mathbf{u}\cdot\nabla c=D\nabla^2 c. \tag{3}$$

Our Darcy's law approach reduces the three-dimensional flow $\mathbf{v}(x,y,z)$ to an equivalent two-dimensional flow $\mathbf{u}=\mathbf{u}(x,y)$ by averaging over the "gap" direction (or equivalently, along the z axis) such that $\mathbf{u}(x,y)=\int_0^b\mathbf{v}(x,y,z)dz/b$. Equation (1) expresses the gap averaged incompressibility condition. A generalized Darcy's law is expressed by Eq. (2) where p is the hydrodynamic pressure, $\mathbf{r}$ is the position vector, and Q is the additional pressure due to the Korteweg stresses [23,27]. The concentration of the fluid 1 is repre-

sented by c, and $\hat{\delta}$ is the Korteweg stress coefficient. The superscript T denotes a transpose. The concentration equation is given by Eq. (3), where D is the constant diffusion coefficient. As is common in these systems, the Coriolis force can be neglected [2,12].

The viscosity and density variations of the mixture are assumed as [44,45]

$$\eta(c) = \eta_1 \exp[\mathcal{R}(1-c)], \tag{4}$$

$$\rho(c) = c\rho_1 + (1-c)\rho_2, \tag{5}$$

where $\mathcal{R}=\ln(\eta_2/\eta_1)$ is a viscosity parameter. In order to render the governing equations dimensionless, the diameter of the initially circular interface $2R$ and the density difference $\Delta\rho=(\rho_2-\rho_1)$ are taken as the characteristic scales. We further scale the viscosity and time with η_1 and $(12\eta_1/b^2\Delta\rho\Omega^2)$, respectively. In conjunction with a characteristic pressure $4\Delta\rho\Omega^2R^2$, dimensionless parameters, such as the viscosity contrast A, the rotational Péclet number Pe and the Korteweg constant δ are defined as

$$A = \frac{\eta_2-\eta_1}{\eta_2+\eta_1}, \quad \mathrm{Pe} = \frac{\Delta\rho\Omega^2b^2R^2}{3\eta_1 D}, \quad \delta = \frac{\hat{\delta}}{16\Delta\rho\Omega^2R^4}. \tag{6}$$

The dimensionless governing equations can be rewritten in terms of stream function (ϕ) and vorticity (ω) formulation as [13,23,45]

$$\nabla^2\phi = -\omega, \tag{7}$$

$$\omega = -\mathcal{R}\,\boldsymbol{\nabla}\phi\cdot\boldsymbol{\nabla}c - \frac{1}{\eta}\left[y\frac{\partial c}{\partial x} - x\frac{\partial c}{\partial y}\right] - \frac{\delta}{\eta}\left[\frac{\partial c}{\partial x}\left(\frac{\partial^3 c}{\partial x^2\partial y} + \frac{\partial^3 c}{\partial y^3}\right) - \frac{\partial c}{\partial y}\left(\frac{\partial^3 c}{\partial x\partial y^2} + \frac{\partial^3 c}{\partial x^3}\right)\right], \tag{8}$$

$$\frac{\partial c}{\partial t} + \mathbf{u}\cdot\boldsymbol{\nabla}c = \frac{1}{\mathrm{Pe}}\nabla^2 c. \tag{9}$$

In addition, the boundary conditions are prescribed as

$$x \text{ direction:} \quad \phi = 0, \quad \frac{\partial c}{\partial x} = 0, \tag{10}$$

$$y \text{ direction:} \quad \phi = 0, \quad \frac{\partial c}{\partial y} = 0. \tag{11}$$

In order to reproduce the very fine structures of the fingers successfully, a highly accurate spectral method is applied. As a result, the actual boundary conditions applied in the numerical codes at x direction are modified as $\partial\phi/\partial x=0$. The above conditions automatically lead to $\phi=0$ under the situation where no concentration gradient is generated on these boundaries before the calculations terminated. The initial conditions assume a circular droplet shape bounded by a steep concentration gradient in a form of error function. To break the unphysical artificial symmetry, a small magnitude of random noises is applied to the positions of 0.5 concentration. To solve the stream function by a pseudospectral method, a Galerkin-type discretization using cosine expansion is employed in the x direction both on ω, and ϕ. In the y direction, discretization is accomplished by sixth order compact finite differences. The vorticity ω is evaluated using a compact finite difference scheme by summing up numerically all the terms on the right hand side of Eq. (8). A fully explicit third order Runge-Kutta procedure on time and spatial sixth order compact finite difference schemes are employed to solve the concentration. The set of equations is then solved and advanced in time. The numerical code is similar to the one used for earlier investigations of miscible flow in other geometries [13,27,29,45], and is quantitatively validated by comparing the growth rates with the values obtained from the linear stability theory in a plane front. We refer the reader to the original studies [45–47] for more details on the implementation and quantitative validation of these numerical schemes.

We close this section by pointing out some important requirements and limitations of the Darcy's law formulation we employed in this work. An important requirement refers to the fact that the velocity profile across the gap needs to remain parabolic [38,43,48–55]. For the cases of forced flow with sufficiently high Péclet number, defined as $\mathrm{Pe}_f=Ub/D$, where U denotes a characteristic flow velocity, a wetting layer is formed on the walls of the cell while narrower fingers grow in the central regions of the gap [38,43,48–50]. This defines a three-dimensional fingering problem, indicating that the assumption of parabolic velocity profile no longer holds. So, for such high Péclet number regime the gap-averaged Darcy's approach is no longer valid. Recent results in density-driven flows [52–55] also show that for high-Rayleigh numbers $\mathrm{Ra}=\Delta\rho g b^3/(12\eta_1 D)$ (this parameter is indeed a Péclet number), where g represents the acceleration of gravity, similar wetting problems occur so that the Hele-Shaw equations might not be able to provide a completely accurate description of the flow field. Under these situations (high Pe_f or high Ra limits), the full three-dimensional Stokes equations or Brinkman model seem to be more appropriate and accurate. However, it has been shown in Refs. [43,49,50,53,54] that, if the magnitudes of Pe_f and Ra are no larger than certain values [$\mathrm{Pe}_f \sim O(10^4)$ and $\mathrm{Ra} \sim O(10^2)$] the physical problem is still accurately described by a conventional Darcy's model. A more detailed review regarding the validity of Darcy's model for such miscible flows can be found in Refs. [53,54]. It is worth noting that even though the fully three-dimensional Stokes equations are able to accurately catch a whole range of miscible fingering situations, its numerical implementation is considerably challenging and difficult. Therefore, the well developed and highly accurate numerical schemes applicable to the conventional Darcy's model is a very welcome and useful tool for exploring the current miscible rotating Hele-Shaw problem.

Considering the restrictions on the Darcy's law approach described in the previous paragraph, we need to be absolutely certain that the values of the Péclet numbers we use in our simulations [see Eq. (6)], lie within the required low Pe_f and low Ra regimes. Since to date there are no experimental studies of *miscible* fingering in rotating Hele-Shaw cells with which the current theory can be more directly compared, we rely on the well established requirements on the values of the

Péclet numbers for the rectilinear forced and density-driven flows discussed above to estimate equivalent restrictions for our current problem. Notice that the main difference between the definitions of the rectilinear parameters Pe_f and Ra, and our rotating flow Péclet number Pe is basically the length scale, in the sense that the rectilinear effects are mainly determined by the gap width b, while here we consider the droplet diameter $2R$ as a characteristic length scale. Recalling that in our rotating case $U=\Delta\rho\Omega^2 b^2 R/(12\eta_1)$, and after appropriate rescaling, it can be shown that the magnitude of our Pe is typically larger than the ones of the Péclet numbers Pe_f and Ra by a factor proportional to the ratio of the droplet diameter by the gap width, i.e., $\mathrm{Pe}\sim(R/b)\mathrm{Pe}_f$ [and $\mathrm{Pe}\sim(R/b)\mathrm{Ra}$]. We conclude that in order to fall within the required low Pe_f and low Ra regime, we need to be sure that we consider a sufficiently large ratio R/b for our rotating Hele-Shaw system. So, for typical values of $R/b\sim 10^2$ commonly used in rotating immiscible Hele-Shaw flow experiments [2,11,12], the upper bound for our Péclet number that safely meets the requirements of validity for the Darcy's law approach would be $\mathrm{Pe}\leqslant O(10^4)$. This is exactly in the range of values for Pe we simulated here, ensuring the applicability and reliability of the Darcy's law formulation in accurately describing our current physical problem. This claim is additionally reinforced by the fact that our miscible numerical simulations compare quite well with the immiscible patterns found in Ref. [12], when the effects of Korteweg stress (effective surface tension) are introduced. Indeed, as one can verify in the next sections, we go beyond this "visual" (somewhat qualitative) comparison between miscible and immiscible patterns by means of the concept of the effective surface tension which allow us, on the other hand, to make more quantitative predictions and estimate the number of rising fingering structures quite accurately.

III. RESULTS AND DISCUSSION

The main results and discussions of our study are divided in two separate parts. In Sec. III A we examine the influence of viscosity contrast and Korteweg stresses on the development of fingering instabilities in miscible rotating Hele-Shaw flow. We explore the richness of the miscible system, and obtain a vast variety of pattern morphologies as the main physical parameters (A, Pe, and δ) are changed. The response of the finger competition behavior to these changes is studied in detail, and many interesting interfacial features are properly identified and discussed. In particular, a suggestive connection between the miscible and immiscible situations is qualitatively obtained for larger values of Korteweg stresses. In Sec. III B we perform a more quantitative study, and define a control parameter, the so-called miscible effective interfacial tension, which is the miscible equivalent of the usual immiscible surface tension. Our approach allows the determination of a quantitative relationship between the number of fingers formed in fully nonlinear stages and the miscible effective interfacial tension. Finally, our numerical results for miscible rotating flows are systematically compared to simulations and experiments performed in its immiscible counterpart.

A. Qualitative analysis: Influence of viscosity contrast and Korteweg stresses

It has been recently reported [6,12,16] that pattern morphology and finger competition dynamics for immiscible flow in rotating Hele-Shaw cells depend strongly on the viscosity contrast. In this section we investigate how finger competition and the shape of the emerging patterns behave under miscible circumstances. The combined role of viscosity contrast A, Péclet number Pe, and Korteweg stresses δ in determining the mixing interface evolution is systematically studied, and a useful parallel between immiscible and miscible cases is found. We identify the basic morphological features of the mixing interface as larger Korteweg stresses are introduced, and verify if the miscible patterns obtained present a better resemblance to their immiscible counterparts as δ is increased.

We begin our analysis (see Fig. 2) by focusing on the case in which the inner fluid is less viscous, so that the viscosity contrast is large and *negative* ($A=-0.905$). Recall that the equivalent immiscible situation resulted in patterns presenting a series of petal-like structures, in which the outward fingers are considerably wider at the tips, and tend to pinch off at the bottom, in a region near the rotation axis [16]. For the immiscible case it is also detected a strong finger length variability of outward fingers (characterizing a strong competition among them), while the inward moving fingers of the outer fluid do not compete as much.

Figure 2 presents numerical simulations for the miscible case with $A=-0.905$ and $\mathrm{Pe}=10^3$. It illustrates the effects of increasingly larger Korteweg stress parameter δ on the evolution of the patterns. The rows in Fig. 2 are arranged according to the value of δ: top row (a)–(c) for $\delta=0$; middle row (d)–(f) for $\delta=-5.0\times10^{-6}$; and bottom row (g)–(i) for $\delta=-10^{-5}$. Notice that throughout this work we use only negative values for δ. As pointed out in Ref. [23], a meaningful interpretation of Korteweg stresses as an effective surface tension in Hele-Shaw flows requires the use of negative values of δ, otherwise the problem would be ill posed. In each row time advances from left to right($t=0.5$, 1.0, and 1.25). When $\delta=0$ miscible viscous fingering patterns arise as the mixing front evolves, characterized by finger competition, merging and shielding [see Figs. 2(a)–2(c)]. The most peculiar morphological aspect of the patterns is the fact that while the fingers of the less viscous fluid move outward due to centrifugal driving, they remain relatively wide, and their tips become more blunt. In addition, one observes very strong finger competition (or, finger length variability) among the outward fingers of the less viscous fluid. This interfacial behavior is reminiscent of the usual Saffman-Taylor instability [19] occurring in immiscible fluids (less viscous fluid displacing a more viscous one), indicating it is primarily determined by a viscosity driven mechanism even in the current miscible case. As δ is increased [Figs. 2(d)–2(f) and Figs. 2(g)–2(i)] the stabilizing role of the Korteweg stresses is revealed, and the typical number of fingers is decreased. Another noteworthy effect of δ refers to its influence on the shape of the fingers: as δ is increased the outward fingers become less elongated, and their fingertips widen assuming more rounded shapes. Although the number

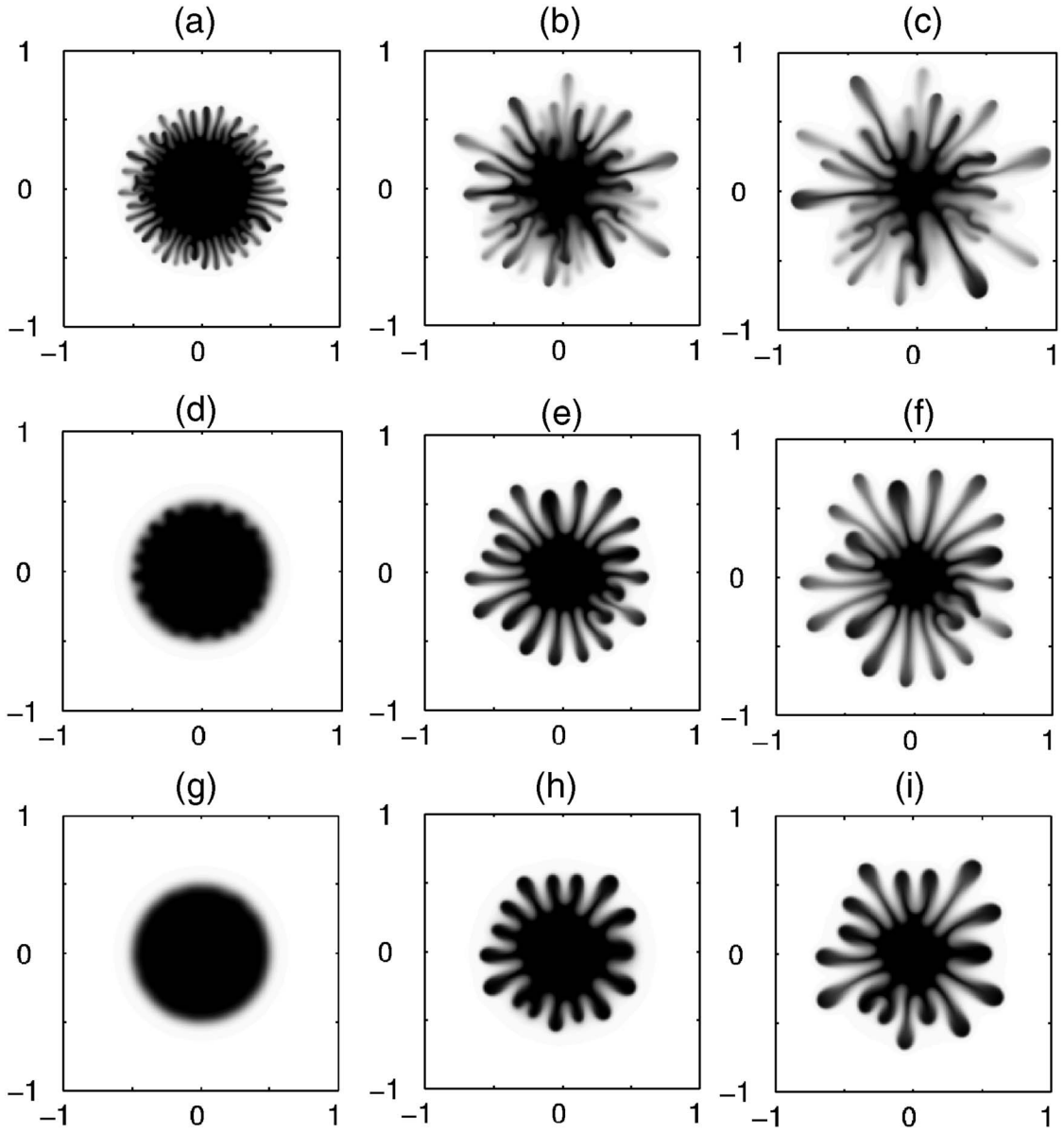

FIG. 2. Images of concentration fields for $A=-0.905$ (darker fluid is less viscous) and $\mathrm{Pe}=10^3$, at $t=0.5$, 1.0, 1.25 (a)–(c) $\delta=0$, (d)–(f) $\delta=-5.0\times10^{-6}$, and (g)–(i) $\delta=-10^{-5}$.

of fingers is decreased for larger δ, finger competition between outward moving fingers is still quite evident for all patterns presented in Fig. 2. Also note that the central droplet region is somewhat "preserved," exhibiting increasing circularity for the largest value of δ. This would indicate weak competition among more viscous fingers moving inward. As a matter of fact, for the case of strongest Korteweg stresses simulated in Figs. 2(g)–2(i), the fingering patterns do resemble the ones obtained by numerical simulations of the equivalent immiscible situation with $A=-1$ [16]. Since experiments for negative A are still inexistent in rotating Hele-Shaw cells, the similarity between our current miscible results for higher magnitude of δ and $A<0$ [Fig. 2(i)], and the immiscible patterns simulated for $A=-1$ in Ref. [16] (using a completely different numerical and theoretical approach) is a good indication, pointing to the correctness and accuracy of both numerical studies.

We proceed by analyzing the case in which the viscosities of the fluids match, so that $A=0$ (Fig. 3). As discussed in the analysis of Fig. 2 for the case of negative viscosity contrast, a less viscous rotating drop tends to destabilize the outward growing fingers, but stabilizes the inward penetrating fingers. On this basis, we should not expect strong length variability of both the outward and inward fronts if the droplet and surrounding fluid present similar viscosity values. To test the validity of this hypothesis in the miscible case we plot in Fig. 3 the patterns for $A=0$ and $\mathrm{Pe}=10^4$, assuming the same values of the Korteweg stress parameter δ used in Fig. 2. In order to obtain a similar degree of fingering as the one produced in Fig. 2, here we use a higher value of Pe to compensate the fact that $A=0$. A higher Péclet number means weaker diffusion effects or stronger centrifugal driving. In each row of Fig. 3 time advances from left to right ($t=2.5$, 3.5, and 4.5). When $\delta=0$ [Figs. 3(a)–3(c)] very vigorous fin-

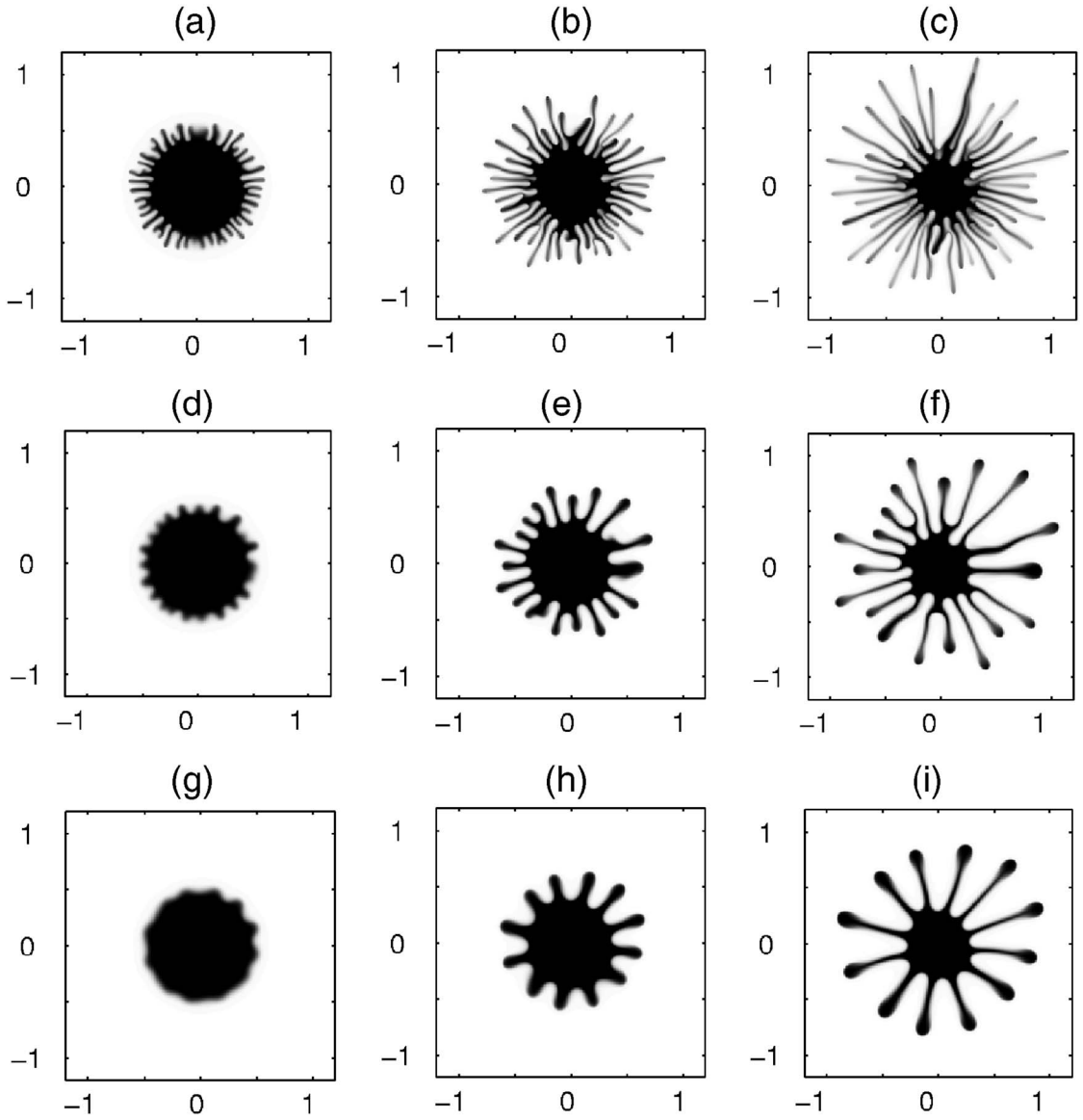

FIG. 3. Images of concentration fields for $A=0$ (viscosity-matched fluids) and $\mathrm{Pe}=10^4$, at $t=2.5$, 3.5, 4.5 (a)–(c) $\delta=0$, (d)–(f) $\delta=-5.0\times10^{-6}$, and (g)–(i) $\delta=-10^{-5}$.

gering is observed, resulting in the development of numerous fingers, which are much thinner than those produced in Figs. 2(a)–2(c). This is justified by the fact that higher Pe leads to smaller dispersion which prevents transverse diffusion, resulting in thinner fingers. Moreover, as the centrifugal force is proportional to the radial distance and $A=0$, the fingers of the inner fluid tend to move radially outward, getting thinner and thinner as time progresses. Finger competition is also present, mainly between the outward moving fingers. As the Korteweg stress parameter is introduced [Figs. 3(d)–3(f) and Figs. 3(g)–3(i)] things start to change significantly. When $\delta=-5.0\times10^{-6}$ [Figs. 3(d)–3(f)] we obtain patterns that present a smaller number of relatively thicker fingers, which tend to stretch, resulting in structures with long necks and bulbous ends. However, finger competition among outward moving fingers is still quite evident in Figs. 3(d)–3(f). On the other hand, if δ is increased further [Figs. 3(g)–3(i)] the outward fingers present almost the same lengths, indicating that the competition among them has been almost completely suppressed. It is also observed in Figs. 3(g)–3(i) that the central region of the droplet delineates a nearly circular inner mixing front, indicating that the competition among the penetrating fingers of the outer fluid is severely restrained. We point out that the fingering patterns obtained in Figs. 3(g)–3(i) for larger δ (thin filaments connected to relatively large droplets located at their tips) are extremely similar to the simulated immiscible fingers for the case $A=0$ [16].

We conclude by presenting the case in which the inner fluid is much more viscous than the outer one, so that the viscosity contrast is large and *positive*, or $A=0.905$. Here we increase the value of the Péclet number even further (now $\mathrm{Pe}=2.0\times10^4$) in order to overcome the stabilizing role of large and positive viscosity contrast, and get patterned structures presenting branching and complexity similar to the ones shown in Figs. 2 and 3. In addition, to get fully developed fingers we had to run our simulations to sufficiently

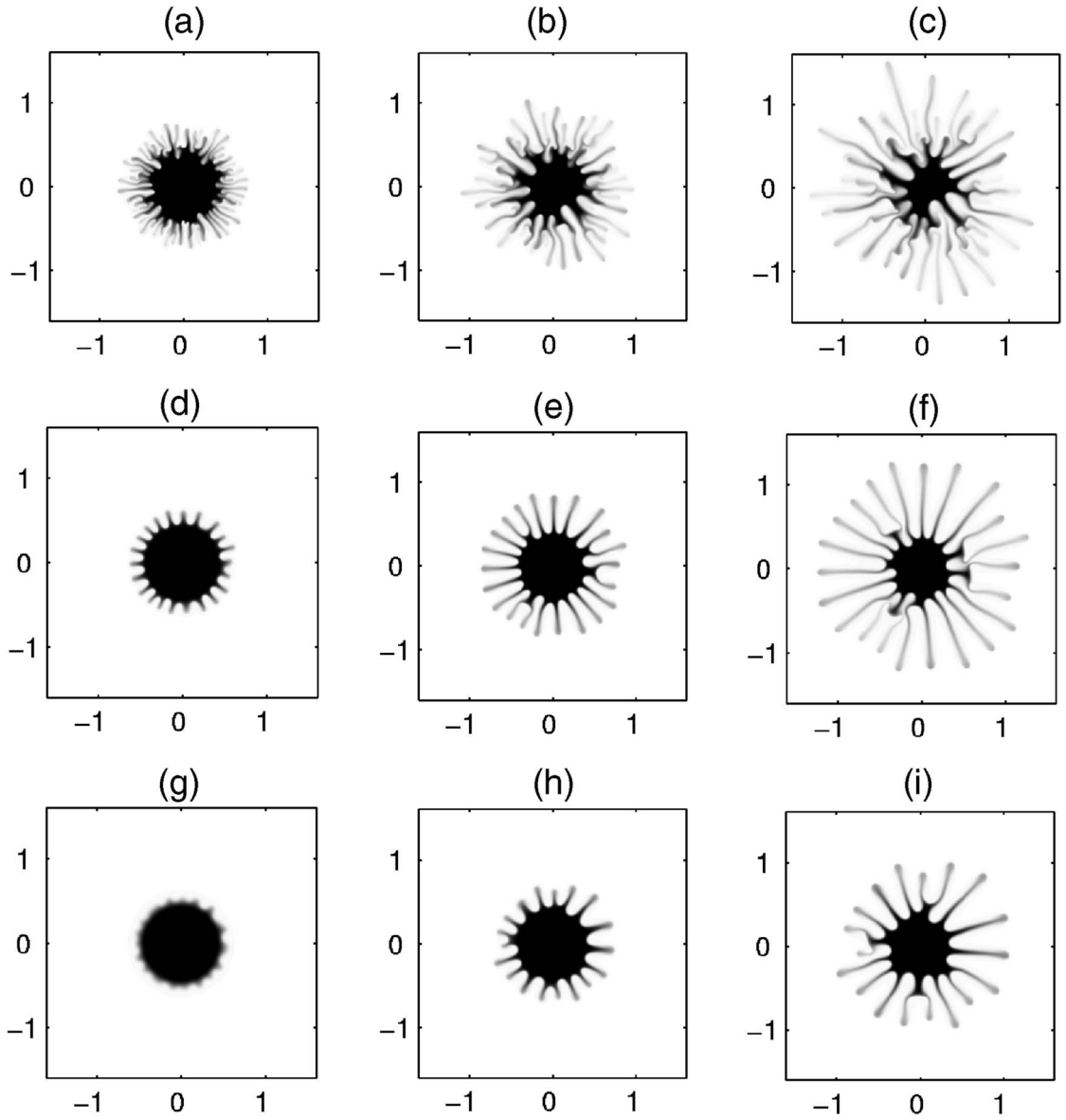

FIG. 4. Images of concentration fields for $A=0.905$ (darker fluid is more viscous) and $\mathrm{Pe}=2.0\times10^{4}$, at $t=10$, 15, 20 (a)–(c) $\delta=0$, (d)–(f) $\delta=-5.0\times10^{-6}$, and (g)–(i) $\delta=-10^{-5}$.

long times: $t=10$ (first column), $t=15$ (second column), and $t=20$ (third column) in Fig. 4. The values of δ are the same as the ones used in Figs. 2 and 3. The concentration images depicted in Fig. 4 show that the use of large and positive A alters the fingering patterns dramatically. When Korteweg stresses are totally absent [see Figs. 4(a)–4(c) for $\delta=0$] the resulting pattern is highly branched and fragmented. The elongated fingers of the inner fluid are very thin, and appear in a variety of lengths. Actually, the fingers observed in Fig. 4 are generally thinner than the previous two cases illustrated in Figs. 2 and 3. Moreover, the internal region of the inner fluid is quite irregular, being clearly invaded by the penetrating fingers of the outer less viscous fluid. Here the inward penetrating fingers of the less viscous fluids are unstable and tend to advance towards the center of the inner droplet. As a result, a more irregular inner front is observed caused by the stronger competition among inward moving fingers. Conversely, the outward moving fingers of the more viscous fluid face a strong dispersion due to local stabilizing viscous effects. Figures 4(d)–4(i) illustrate how δ influences the behavior of the mixing interface. Generally speaking, it is clear that the number of fingers is decreased and that the competition among them is restrained, markedly the competition among outward moving fingers of the more viscous fluid. The morphology of the outward fingers is also evidently changed, and now the width of these fingers remain approximately constant along their lengths, so that the inner fluid does not accumulate at the tip of the fingers. This is in striking contrast to the behavior of the fingers depicted in Figs. 2(g)–2(i) and 3(g)–3(i). Once again, the miscible patterns we show in Figs. 4(g)–4(i) are quite similar to those obtained in experiments with prewetted cells [11,12] and numerical simulations [11,12,16] for the immiscible flow case with $A=1$.

B. A more quantitative analysis: The miscible effective interfacial tension

Based on our results discussed in Sec. III A, two important qualitative findings are verified: (i) for the entire range of values of the viscosity contrast A (negative, positive, or null), our numerical simulations for *miscible* flow in rotating Hele-Shaw cells reproduce accurately the typical fingering patterns obtained in the corresponding immiscible case, if the relevant miscible parameters δ and Pe are properly chosen; (ii) Korteweg stresses do introduce surface tensionlike effects, in the sense that increasingly larger magnitudes of δ clearly lead to stabilizing effects and reduction in fingering. In the search for a more quantitative characterization of the behavior of Korteweg stresses in miscible flows, and its relation to ordinary immiscible surface tension σ, one interesting question arises: is it possible to define an effective miscible interfacial tension parameter which is more directly linked to its immiscible counterpart? Our main purpose in this section is to try to answer this question as quantitatively as possible.

We use our numerical approach to carry out a systematic, and more direct quantitative comparison between miscible and immiscible flow fields. We perform our comparative study by contrasting our miscible results with an interesting and accurate investigation recently executed by Alvarez-Lacalle *et al.* [12]. In Ref. [12] the immiscible flow in rotating Hele-Shaw cell is studied in detail (both analytically, numerically, and experimentally) in situations of relatively low A ($A \approx 0.4$) and small values of σ. Under such circumstances, it has been found the development of fingering structures characterized by fingers which grow radially outwards and stretch, becoming gradually thinner, to a point that fingers pinch off and emit droplets. Their numerical simulations for the immiscible case (based on a boundary integral approach) show excellent agreement with their experimental findings. Another relevant result obtained in Ref. [12] is the connection between the typical number of emerging fingers N with a dimensionless surface tension parameter S

$$N \approx \sqrt{\frac{S}{3}}, \tag{12}$$

where

$$S = \frac{\Delta \rho R^3 \Omega^2}{\sigma}. \tag{13}$$

They have shown that, due to the restrained finger competition, the typical number of fingers obtained experimentally matches the theoretical prediction given in Eq. (12) even in the deeply nonlinear regime. We point out that Refs. [6,16] use an equivalent definition for the dimensionless surface tension parameter given as $B=1/S$.

In order to implement an important part of our quantitative comparison, we follow Chen *et al.* [31] and define a dimensionless *miscible* effective interfacial tension parameter S_m, by replacing the immiscible surface tension σ appearing in Eq. (13) by a miscible effective interfacial tension [25,31,56] such that

$$S_m = \frac{1}{8\sigma_{EIT}}, \tag{14}$$

where

$$\sigma_{EIT} = \int_M |\delta| \left(\frac{dc}{dn}\right)^2 dn, \tag{15}$$

is the *dimensionless* miscible effective interfacial tension. In Eq. (15) the integration is taken across (and perpendicularly to) the mixing interface (n represents the normal direction to the interface), with M denoting the mixing region. Notice that the integrand in Eq. (15) is reminiscent of the Korteweg stress contribution appearing as the third term at the right hand side of the generalized Darcy's Law [see Eq. (2)]. So, the miscible effective surface tension is naturally defined by integrating such squared normal gradient of the concentration across the interface. With this definition in our hands and by analogy with Eq. (12), we propose an explicit expression for the number of fingers produced in the *miscible* case

$$N_m \approx \sqrt{\frac{S_m}{3}}. \tag{16}$$

One way of testing the usefulness and correctness of the miscible expressions for N_m and S_m is to evaluate them numerically, simulate the miscible fingering patterns, and compare these structures with the equivalent immiscible patterns produced by using the corresponding values for N and S given by Eqs. (12) and (13). By validating the expressions for N_m and S_m we will provide an important quantitative evidence for the claim that (after appropriate reintroduction of dimensions) σ_{EIT} not only acts as its immiscible counterpart σ, but it is in fact the equivalent quantity to be considered in miscible situations. We point out that, for a constant value of A, Eq. (15) is a function of both δ and Pe (of course, concentration profile depends on the Péclet number). So, by using σ_{EIT} the number of dependent variables in the problem is conveniently reduced to one.

Before continuing the investigation of this more quantitative section, we briefly discuss a practical aspect, related to the typical order of magnitude of the effective surface tension and Korteweg stress parameters measured in experiments and predicted by other theoretical studies. Here we relate these findings to the typical values of the equivalent parameters we use in our current numerical simulations, and show they are quite consistent. There have been numerous attempts in the literature to obtain the values of the effective interfacial tension. For instance, the interfacial tension of ethyl alcohol with a salt solution is measured between 8.0×10^{-1} and 3.0×10^{-3} N/m [35,36]. A maximum surface tension value of 10^{-3} N/m at the time of initial contact between silicone oils of 1 and 2000 cSt are reported in Ref. [37]. Analogy between the miscible and immiscible capillary tube experiments, an effective surface tension value between glycerine and water of about 5.0×10^{-4} N/m is suggested [38]. Based on theoretical arguments, Davis [25] calculates values for mixtures of hydrocarbons up to 10^{-4} N/m. By the experiments on a spinning drop tensometery [39] another value of surface tension 5.8×10^{-4} N/m between water and

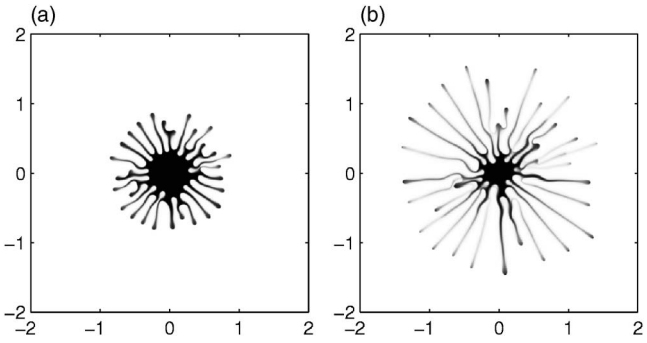

FIG. 5. Images of concentration fields for $\mathrm{Pe}=1.5\times10^4$, $A=0.4$ (darker fluid is more viscous), and $\delta=-1.7\times10^{-6}$ at (a) $t=5.0$, and (b) $t=7.5$. The correspondent mean miscible effective interfacial tension parameter is at about $S_m=2575$ with the number of fingers $N_m=29$.

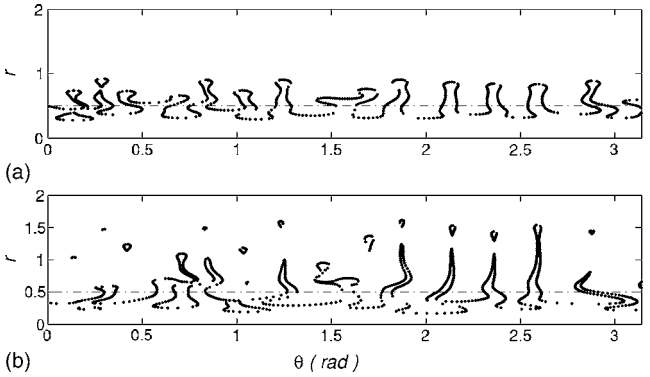

FIG. 6. Polar representation(r vs θ) of the interfaces shown in Fig. 5 for concentration contours of $c=0.65$, $\mathrm{Pe}=1.5\times10^4$, $A=0.4$, and $\delta=-1.7\times10^{-6}$ at (a) $t=5.0$ and (b) $t=7.5$. The initial condition is represented by the dashed-dotted straight line. Lack of strong finger competition can be verified in (a), while the droplet emission phenomena is clearly seen in (b).

glycerine is observed. Although one cannot predict the value of the effective surface tension σ_{EIT} *solely* from the value of the Korteweg stress parameter (σ_{EIT} is concentration dependent), we can certainly estimate the value of the *dimensional* effective surface tension $\hat{\sigma}_{EIT}\sim\Delta\rho\Omega^2R^3/S_m$ we used, and compare them with the ones mentioned above. For the experimental conditions ordinarily present in immiscible rotating Hele-Shaw experiments [2,11,12], i.e., $\Omega=150$ rpm, $R=25$ mm, $\Delta\rho=100$ kg/m^3, and $50\leqslant S_m\leqslant3000$ we obtain a dimensional effective surface tension $O(10^{-3})$ N/m$\leqslant\hat{\sigma}_{EIT}\leqslant O(10^{-2})$ N/m. This reflects the good agreement between the values we use in our simulations, and the ones measured in Refs. [25,35–39]. As to the typical values of the Korteweg constant, an estimate of $10^{-11}\leqslant\hat{\delta}\leqslant10^{-8}$ N for polymer solvent is reported in Ref. [32]. If we take this estimate for $\hat{\delta}\sim O(10^{-10}-10^{-9})$ N, and again apply it into the ordinary conditions of immiscible rotating Hele-Shaw experiments [2,11,12], we obtain a dimensionless $\delta\sim O(10^{-6}-10^{-5})$. We point out that values of δ used in our simulations are absolutely consistent with the typical magnitudes of δ mentioned above [32]. One last point about δ refers to its sign: when formulating the gap averaged equations that account for Korteweg stress in Hele-Shaw flows, it is found the constant δ has to have a negative value in order to avoid the so-called Hadamard instability, which would make the problem ill posed. This requirement on the sign of δ has been extensively verified (see for instance, Refs. [27,28]), and it is not a simple mathematical condition, but rather an important physical requirement imposed on δ in order to allow it to act similarly to an ordinary surface tension. A more detailed account about this last point can be found in Refs. [23,24].

We begin our more direct comparisons by performing a series studies of the concentration images obtained from different values of the Korteweg stress δ. Hereinafter, we assume that $A=0.4$ in order to match the viscosity contrast used in immiscible experiments and simulations presented in Ref. [12]. Figure 5 depicts the snapshots of concentration images for a representative case with $\mathrm{Pe}=1.5\times10^4$ and $\delta=-1.7\times10^{-6}$. At time $t=5$ we observe the formation of fingering patterns which compete mildly, characterized by the development of thin fingers, which eventually form forklike structures. As time progresses ($t=7.5$) the fingers stretch radially, becoming very thin. Denser concentration accumulation is found at the finger tip area. It is interesting to point out that the fingering pattern depicted in Fig. 5(a) presents a striking similarity with the experiments and simulations of Ref. [12]. We urge the reader to check this last point, by comparing the miscible pattern shown in Fig. 5(a) with the immiscible interfacial shapes illustrated in Figs. 3 and 20 of Ref. [12]. It is evident that all the main fingering features present in the immiscible case, such as the suppressed finger competition, the existence of forklike structures, the emergence of droplets at the fingertips, and even the typical number of fingers formed ($N_m\approx29$) are well reproduced in Fig. 5(a).

Another peculiar feature of the immiscible patterns is the occurrence of droplet emissions at the end of the thin fingers [12]. Even though apparent droplet emissions at the fingertips are hard to identify on the images of concentration fields shown in Fig. 5, they are clearly visible in the equivalent polar representation of the interface illustrated in Fig. 6. Figure 6 plots the dimensionless radius r of the mixing interface shown in Fig. 5 as a function of the polar angle θ, by taking the concentration contour with $c=0.65$. Again, the polar representation of the miscible interface is very similar to the one obtained in the corresponding immiscible experiment (see Fig. 4 in Ref. [12]). By examining Fig. 6 we confirm that outward fingers compete weakly [Fig. 6(a)], while droplet emission does occur at the end of the fingers [Fig. 6(b)]. It is worthwhile to note that the droplet detachment phenomena detected in the current miscible case (Fig. 6) are attributed to slightly different physical mechanisms from those associated to the phenomena of droplet emission in immiscible flows. While the emission in immiscible situations indicates the occurrence of interfacial singularities [12], it happens much more smoothly in miscible cases due to diffusive effects. As a result, this interesting morphological aspect can be accurately simulated much more easily under miscible circumstances [33].

In order to further validate the surface-tensionlike effects of miscible effective interfacial tension, we simulate miscible

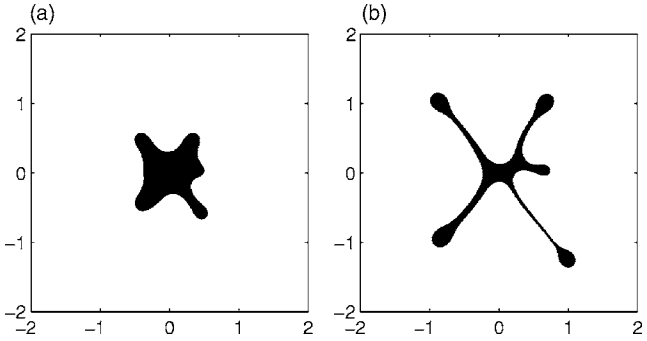

FIG. 7. Images of concentration fields for $\mathrm{Pe}=1.5\times10^4$, $A=0.4$ (darker fluid is more viscous), and $\delta=-6.5\times10^{-5}$ at (a) $t=9.0$ and (b) $t=12$. The correspondent miscible effective interfacial tension parameter is at about $S_m=92$ with the number of fingers $N_m=5$.

patterns with an even stronger Korteweg constant, and compare them with the corresponding immiscible patterns generated for larger immiscible surface tension. These immiscible patterns can be found in the right panel of Fig. 20 in Ref. [12]. Figure 7 shows the concentration images for the immiscible situation with $\mathrm{Pe}=1.5\times10^4$, $\delta=-6.5\times10^{-5}$, and times $t=9$ and 12. As one can observe, the similarity between the miscible patterns depicted in Fig. 7 and the immiscible ones shown in Fig. 20 in Ref. [12] is quite remarkable. Both the general shape and the number of fingers formed ($N_m=5$) are very accurately matched.

At this point, it is worth mentioning that unlike the global immiscible surface tension, the dimensionless miscible effective interfacial tension σ_{EIT} [Eq. (15)] is a local parameter with temporal and spatial dependence on the concentration distribution. Consequently, no global values of dimensionless miscible effective interfacial tension parameter S_m really exist. With this in mind, we now describe a way to get a reasonable and reliable average value for S_m. We consider the interfacial area in the x-y plane, and take four particular locations as representative. Figure 8 plots the time evolution of these four representative values of S_m, and their mean values,

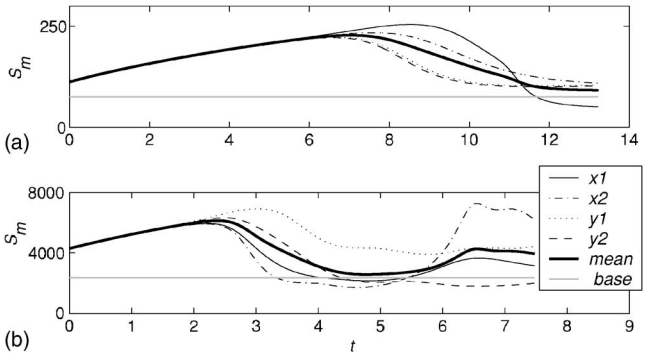

FIG. 8. Time evolution of the miscible effective interfacial tension parameters of S_m, for $\mathrm{Pe}=1.5\times10^4$, $A=0.4$, and (a) $\delta=-6.5\times10^{-5}$ and (b) $\delta=-1.7\times10^{-6}$. The lines $x1$, $x2$ indicate the values obtained along the x axis, and $y1$, $y2$ are calculated along the y axis. The solid black curves represent the time evolution of the mean values of S_m (see text). The theoretical base values are represented by gray straight lines: (a) $S_{base}=75$ and (b) $S_{base}=2325$.

for the cases shown in Figs. 5 and 7. The curves $x1$, $x2$ indicate the values obtained for S_m along the x axis, and $y1$, $y2$ are ones calculated along the y axis. The mean value of S_m is obtained by simply considering the arithmetic mean of its four values taken at $x1$, $x2$, $y1$, and $y2$ for a given time. Initially, in Fig. 8, these four representative miscible effective interfacial tension parameters S_m show an early growth determined by the initial conditions. As shown in Fig. 8(a) for relatively simple fingering patterns with stronger effective interfacial tensions, such as $\delta=-6.5\times10^{-5}$, the four representative values of S_m all converge to their mean value and remain nearly constant. This nearly constant mean value is found at about $S_m=92$ as shown Fig. 8(a). Regarding the situation with weaker interfacial tension at $\delta=-1.7\times10^{-6}$ shown in Fig. 8(b), we observe that the establishment of a time period for which S_m is nearly constant is not possible after $t\approx6$. This is mainly caused by the development of very vigorous fingering (as shown in Fig. 5): the strong dispersion associated with complex fingering patterns prohibits an accurate evaluation for σ_{EIT}. Nevertheless, a nearly constant mean value for S_m still can be defined for the time interval between the $4<t<6$, prior the occurrence of more dramatic interfacial deformations. This value is estimated at about $S_m=2575$ in Fig. 8(b). The gray straight lines shown in Fig. 8 refer to the theoretical base value of the known number of fingers defined as $S_{base}=3N_m^2$. By taking the known number of fingers obtained above ($N_m=5$, 29) the corresponding base values in Figs. 8(a) and 8(b) are $S_{base}=75$, 2523, respectively.

As we stated previously, an important goal in this section is to make more direct, quantitative comparisons between our miscible patterns and the ones obtained in immiscible experiments and simulations [12]. One obvious way to do this is to verify the validity of the theoretical expression [Eq. (16)] relating the number of fingers N_m and the miscible effective interfacial tension parameter S_m [Eq. (14)]. By considering the mean values of S_m obtained above, namely $S_m=92$ (Fig. 7) and $S_m=2575$ (Fig. 5), and by substituting these directly into the expression $N_m=\sqrt{S_m/3}$, we obtain that $N_m=5$ and 29, respectively. Interestingly, this is exactly the number of fingers obtained in Ref. [12] which takes $S=80$ and $S=2500$ and uses the corresponding immiscible expression $N=\sqrt{S/3}$ [Eq. (12)]. This reveals an excellent quantitative agreement between our current numerical predictions and the simulated and experimental results for the immiscible case [12]. We have also tested our results for other values of Pe, and verified that a more direct connection between the immiscible surface tension and its miscible counterpart is obtained when Pe is relatively high (but still within the range of validity of our approach), or when S_m is low. This fact is indeed expected since for such Pe the diffusion is less significant, and the mixing layer is narrower. In addition, the mixing layer is supposed to be more sharply defined in a situation of stronger interfacial tension, or a lower S_m. In this context, instead of relying in two parameters (Pe and δ), one could now use σ_{EIT} is a good representation of surface tensionlike effects in confined miscible flows.

The numerical results presented above illustrate our attempt to quantify the possibility of defining an effective surface tension to miscible flows in Hele-Shaw geometry. Of course, despite the good quantitative predictions for the num-

ber of emerging fingers, more quantitative tests (both analytical and experimental) would be required to bring further support for such a concept. A quantitative analysis that could shed some light upon this issue, could be found within the general context of diffuse-interface approaches to Hele-Shaw [57]: it should focus on the linear regime and possibly the weakly nonlinear regime, and could well rely on the simpler rectilinear (gravity driven) Hele-Shaw setup. In this case, the effect of the finite thickness of the miscible interface would then naturally show up in the dispersion relation, and then the validity of the effective surface tension would possibly appear associated to certain length and time scales. In the fully nonlinear regime, one could focus on a single-finger setup, where an effective surface tension could also be derived in a more rigorous fashion, such as for thermal plumes in Hele-Shaw cells [58]. Other existing theoretical models on diffuse-interface Hele-Shaw flows could also be useful. For instance: in the context of phase-field models, Folch *et al.* [59,60] derive a linear dispersion relation for a diffuse interface for arbitrary viscosity contrast and study it numerically. A possibly more physical treatment of the interface is discussed later also theoretically and numerically by Lee *et al.* [61,62]. More recently, Glasner [63] gives an even more general and mathematical treatment of the diffuse-interface approach to Hele-Shaw flows. All these theoretical approaches and tools seem to be good candidates to alternative analyses which could provide more sophisticated quantitative checks for the validity of the concept of a miscible effective surface tension.

IV. CONCLUDING REMARKS

In this work, we have presented highly accurate numerical simulations for miscible flow in a rotating Hele-Shaw cell. We studied the emergence of fingering patterns for the full range of viscosity contrasts ($-1 \leqslant A \leqslant +1$), and investigate morphological changes as the Korteweg stress parameter δ assumes increasingly larger magnitudes. The interplay between A and δ lead to quite different interfacial behaviors, which are properly described and qualitatively explained. One particularly interesting aspect is the fact that the miscible patterns formed become very similar to their immiscible counterparts for higher values of δ. Under such circumstances (large δ), our miscible simulations are strikingly similar to existing experimental and numerical results for immiscible flows in rotating Hele-Shaw cells. Among other things, our results support the claim that Korteweg stress acts as an effective surface tension for miscible fluid systems.

The very good qualitative indications for a close connection between Korteweg stress and usual surface tension stimulated the pursuit for more quantitative results. As a byproduct of our qualitative investigation, we have concluded that important features of the immiscible patterns could be accurately reproduced by properly adjusting the values of both Korteweg constant δ and Péclet number Pe. This suggestive coupling effect between Pe and δ opened up the possibility of obtaining a single parameter that could act legitimately as a miscible interfacial tension. By defining such a miscible effective interfacial tension parameter S_m, we have been able to obtain a quantitative relationship for the total number of fingering structures formed in fully nonlinear stages of pattern development. With the concept of S_m, we systematically compared our numerical results with experiments and simulations recently performed in the corresponding immiscible case. As a result, excellent agreement has been found, not only with respect to morphological aspects of the patterns, but also concerning the validation for the quantitative prediction for the typical number of fingers $N_m \approx \sqrt{S_m/3}$. The success of our theoretical predictions provide good evidence for the fact that the miscible effective interfacial tension S_m is both qualitatively and quantitatively equivalent to its immiscible counterpart. Of course, although our numerical results look promising, they still have to be further validated by other quantitative analytical and experimental studies.

Despite its intrinsic importance and applicability for the purely miscible situation, our current numerical results also serve to substantiate very recent analytical [6] and numerical [16] studies for corresponding immiscible flows in confined rotating systems. The excellent agreement between our results and the findings of Refs. [6,16] in the high Korteweg stress limit provides a convincing evidence for the usefulness of their weakly [6] and fully nonlinear [16] approaches. In addition, it also indicates the effectiveness and accuracy of our current miscible numerical simulations in capturing key physical aspects of the equivalent immiscible problem. Regarding our purely miscible findings, we hope researchers will feel motivated to test the predictions of the theoretical modeling presented in this work.

ACKNOWLEDGMENTS

J.A.M. thanks CNPq (Brazilian Research Council) for financial support of this research through the CNPq/FAPESQ Pronex program, and CNPq PDE Proceeding No. 200045/2005–9. C.-Y.C. thanks the National Science Council of the Republic of China for financial support of this research through Grant No. NSC 93-2212-E-224-006.

[1] L. W. Schwartz, Phys. Fluids A **1**, 167 (1989).
[2] Ll. Carrillo, F. X. Magdaleno, J. Casademunt, and J. Ortín, Phys. Rev. E **54**, 6260 (1996).
[3] J. A. Miranda, Phys. Rev. E **62**, 2985 (2000).
[4] S. L. Waters and L. J. Cummings, Phys. Fluids **17**, 048101 (2005).
[5] E. Alvarez-Lacalle, E. Pauné, J. Casademunt, and J. Ortín, Phys. Rev. E **68**, 026308 (2003).
[6] H. Gadêlha and J. A. Miranda, Phys. Rev. E **70**, 066308 (2004).

[7] V. M. Entov, P. I. Etingof, and D. Ya. Kleinbock, Eur. J. Appl. Math. **6**, 399 (1996).
[8] F. X. Magdaleno, A. Rocco, and J. Casademunt, Phys. Rev. E **62**, R5887 (2000).
[9] D. Crowdy, Q. Appl. Math. **60**, 11 (2002); SIAM (Soc. Ind. Appl. Math.) J. Numer. Anal. **62**, 945 (2001).
[10] E. Alvarez-Lacalle, J. Ortín, and J. Casademunt, Phys. Rev. Lett. **92**, 054501 (2004).
[11] R. Folch, E. Alvarez-Lacalle, J. Ortín, and J. Casademunt, eprint physics/0408092.
[12] E. Alvarez-Lacalle, J. Ortín, and J. Casademunt, Phys. Fluids **16**, 908 (2004).
[13] C.-Y. Chen and S.-W. Wang, Fluid Dyn. Res. **30**, 315 (2002).
[14] C.-Y. Chen and H.-J. Wu, Phys. Fluids **17**, 042101 (2005).
[15] D. P. Jackson and J. A. Miranda, Phys. Rev. E **67**, 017301 (2003).
[16] J. A. Miranda and E. Alvarez-Lacalle, Phys. Rev. E **72**, 026306 (2005).
[17] Ll. Carrillo, J. Soriano, and J. Ortín, Phys. Fluids **11**, 778 (1999).
[18] Ll. Carrillo, J. Soriano, and J. Ortín, Phys. Fluids **12**, 1685 (2000).
[19] P. G. Saffman and G. I. Taylor, Proc. R. Soc. London, Ser. A **245**, 312 (1958).
[20] G. Tryggvason and H. Aref, J. Fluid Mech. **136**, 1 (1983).
[21] D. Joseph, Eur. J. Mech. B/Fluids **9**, 565 (1990).
[22] G. Galdi, D. Joseph, L. Prezisi, and S. Rionero, Eur. J. Mech. B/Fluids **10**, 565 (1991).
[23] H. Hu and D. Joseph, ZAMP **43**, 626 (1992).
[24] D. Joseph, A. Huang, and H. Hu, Physica D **97**, 104 (1996).
[25] H. Davis, *IMA Volumes in Mathematics and Its Applications 11* (Springer, Berlin, 1988).
[26] J. Pojman, Y. Chekanov, J. Masere, V. Volpert, T. Dumont, and H. Wilke, AIAA Aerospace Sciences Meeting, AIAA-2001–0764, January 8–10, Reno, NV (2001).
[27] C.-Y. Chen, L. L. Wang, and E. Meiburg, Phys. Fluids **13**, 2447 (2001).
[28] C.-Y. Chen and E. Meiburg, Phys. Fluids **14**, 2052 (2002).
[29] C.-Y. Chen, Phys. Fluids **15**, 1086 (2003).
[30] I. Kostin, M. Marion, R. Texier-Picard, and V. Volpert, Math. Modell. Numer. Anal. **37**, 741 (2003).
[31] C.-Y. Chen, H.-J. Wu, and L. Hsu, J. Magn. Magn. Mater. **289**, 364 (2005).
[32] N. Bessonov, V. Volpert, J. Pojman, and B. Zoltowski, Microgravity Sci. Technol. **XVII**, 2 (2005).
[33] C.-Y. Chen, C.-H. Chen, and J. A. Miranda, Phys. Rev. E **71**, 056304 (2005).
[34] U. Gerke and E. Meiburg, J. Fluid Mech. (to be published).
[35] G. Quinke, Ann. Phys. **9**, 4 (1902).
[36] H. Freundlich, *Colloid and Capillary Chemistry*, (London, Mathuen, 1926).
[37] P. Smith, T. van De Ven, and S. Mason, J. Colloid Interface Sci. **80**, 302 (1981).
[38] P. Petitjeans and T. Maxworthy, J. Fluid Mech. **326**, 37 (1996).
[39] P. Petitjeans, C. R. Acad. Sci., Ser. IIb: Mec., Phys., Chim., Astron. **322**, 673 (1996).
[40] P. Petitjeans and P. Kurowski, C. R. Acad. Sci., Ser. IIb: Mec., Phys., Chim., Astron. **325**, 587 (1997).
[41] P. Kurowski and C. Misbah, Europhys. Lett. **29**, 309 (1994).
[42] D. Korteweg, Arch. Neerl. Sci. Exactes Nat., Ser. II **6**, 1 (1901).
[43] C.-Y. Chen and E. Meiburg, J. Fluid Mech. **326**, 57 (1996).
[44] C. T. Tan and G. M. Homsy, Phys. Fluids **31**, 1330 (1988).
[45] C.-Y. Chen and E. Meiburg, J. Fluid Mech. **371**, 233 (1998); **371**, 269 (1998).
[46] M. Ruith and E. Meiburg, J. Fluid Mech. **420**, 225 (2000).
[47] E. Meiburg and C.-Y. Chen, SPEJ **5**, 2 (2000).
[48] Z. Yang and Y. Yortsos, Phys. Fluids **9**, 286 (1997).
[49] E. Lajeunesse, J. Martin, N. Rakotomalala, and D. Salin, Phys. Rev. Lett. **79**, 5254 (1997).
[50] E. Lajeunesse, J. Martin, N. Rakotomalala, D. Salin, and Y. Yortsos, J. Fluid Mech. **398**, 299 (1999).
[51] P. Philippe, C.-Y. Chen, E. Meiburg, and T. Maxworthy, Phys. Fluids **11**, 1705 (1999).
[52] J. Fernandez, P. Kurowski, L. Limat, and P. Petitjeans, Phys. Fluids **13**, 3120 (2001).
[53] J. Fernandez, P. Kurowski, P. Petitjeans, and E. Meiburg, J. Fluid Mech. **451**, 239 (2002).
[54] F. Graf, E. Meiburg, and C. Hartel, J. Fluid Mech. **451**, 261 (2002).
[55] N. Goyal and E. Meiburg, J. Fluid Mech. **516**, 211 (2004).
[56] I. Rousar and E. B. Nauman, Chem. Eng. Commun. **129**, 19 (1994).
[57] D. M. Anderson, G. B. McFadden, and A. A. Wheeler, Annu. Rev. Fluid Mech. **30**, 139 (1998).
[58] M. Ben Amar, Phys. Fluids A **4**, 2641 (1992).
[59] R. Folch, J. Casademunt, A. Hernández-Machado, and L. Ramirez-Piscina, Phys. Rev. E **60**, 1724 (1999).
[60] R. Folch, J. Casademunt, A. Hernández-Machado, and L. Ramirez-Piscina, Phys. Rev. E **60**, 1734 (1999).
[61] H.-G. Lee and J. S. Lowengrub, Phys. Fluids **14**, 492 (2002).
[62] H.-G. Lee and J. S. Lowengrub, Phys. Fluids **14**, 514 (2002).
[63] K. Glasner, Nonlinearity **16**, 49 (2003).